Last Glacial Maximum climate in China: a comparison between PMIP simulations and reconstructions

Dabang Jiang[1, 2, *], Xianmei Lang[1], Zhiping Tian[1, 3], and Donglin Guo[1, 3]

1, Nansen–Zhu International Research Centre, Institute of Atmospheric Physics, Chinese Academy of Sciences, Beijing, China

2, Climate Change Research Center, Chinese Academy of Sciences, Beijing, China

3, Graduate University of Chinese Academy of Sciences, Beijing, China

To be submitted

May 2010

*_Corresponding author address_: Dr. Dabang Jiang, Institute of Atmospheric Physics, Chinese Academy of Sciences, P. O. Box 9804, Beijing 100029, China.

Email: jiangdb@mail.iap.ac.cn

Abstract

Using 25 climate models' experiments conducted for the Paleoclimate Modelling Intercomparison Project (PMIP) and available proxy data, this study examines regional climate conditions in the Chinese mainland during the Last Glacial Maximum (LGM, 21,000 calendar years ago). Compared to baseline climate, annual surface temperature during the LGM reduced by 2.00–7.00^{o}C in China, with an average of 4.46^{o}C, in the ensemble mean of all the models. Annual precipitation and evaporation during the LGM were 5–40% less than baseline climate and reduced on average by 20% (0.60 mm/day) and 21% (0.41 mm/day) at the national scale, respectively, on the basis of the results from 15 models, which are chosen in light of the ability of models to simulate the modern precipitation climatology and the availability of evaporation data. Both the geographical distribution and value of changes in surface temperature, precipitation, and evaporation during the LGM varied with the seasons and with the models, particularly at the sub-regional scale. Model-data comparison indicates that the 25 models reproduce successfully surface cooling trend during the LGM, but fail to reproduce its magnitude in the regions of comparison, particularly in Hexi Corridor and North and Northeast China. The simulations with computed sea surface temperatures (SSTs) are in better agreement with proxy estimates of surface temperature than those with prescribed SSTs. On the other side, large-scale LGM-minus-baseline anomalies in annual precipitation minus evaporation agree well, in a qualitative manner, with lake status-based reconstruction of changes in annual water budget in most parts of the Chinese mainland. The simulations with computed (prescribed) SSTs are consistent (inconsistent) with reconstructed wetter conditions in most parts of West China excluding the Qinghai-Tibetan Plateau.

1. Introduction

The Last Glacial Maximum (LGM) is well known as a period of several thousand years around 21,000 calendar years before present. During this time climate conditions were greatly different from those of today, and global surface temperature was estimated to be 4 to 7^{o}C colder than the present day in terms of a variety of proxy data (Jansen et al., 2007). Considerable effort has been made worldwide to examine the response of the climate system to large radiative perturbations stemming from changes in continental ice sheet, vegetation, and concentrations of atmospheric greenhouse gases and dust content during the LGM. In particular, the LGM is a target period within the framework of the Paleoclimate Modelling Intercomparison Project (PMIP) (Joussaume and Taylor, 1995; Braconnot et al., 2007).

A central theme in paleoclimate modelling is the investigation of different climate models' responses to the same or similar forcings, and the differences or similarities of these responses. On the other side, assessing the extent to which simulations are compatible with proxy data is essential for evaluating the validity of climate models and, hence, for improving our knowledge of processes determining the LGM climate. Using the PMIP simulations of the LGM climate, a few model-data comparisons have been performed in the tropics (Pinot et al., 1999; Braconnot et al., 2007; Otto-Bliesner et al., 2009), the North Atlantic, Europe, and western Siberia (Kageyama et al., 2001, 2006), western Europe (Hoar et al., 2004), and the Greenland and Antarctica (Masson-Delmotte et al., 2006). The simulated large-scale spatial patterns of regional climate change have been shown to be consistent with proxy data (Jansen et al., 2007). Also found are the discrepancies between simulations and proxy data in some aspects, such as boreal winter cooling derived from pollen data being underestimated by climate models in

western Europe and the Mediterranean region (Kageyama et al., 2006; Ramstein et al., 2007). These comparisons have greatly advanced our scientific understanding of climate conditions and dynamical mechanisms underlying the LGM climate in the regions of concern.

In the recent decades, a few global and regional climate simulations using atmospheric general circulation models (AGCMs) or regional climate models nested in AGCMs have been conducted to address the East Asian and Chinese climate during the LGM (Wang and Zeng, 1993; Liu et al., 1995; Chen et al., 2001; Yu et al., 2001; Liu et al., 2002; Jiang et al., 2003; Zhao et al., 2003; Zheng et al., 2004; Ju et al., 2007), in which both agreements and disagreements in regional climate change have been noticeable across the models when compared to each other. As such, to what extent results are model-dependent in China is unclear, which stresses the need to integrate output from multiple climate models. In addition, given that earlier AGCM-based simulations are in line with the framework of the phase one of the PMIP and therefore neglected ocean dynamics, and that they underestimate reconstructed changes in surface temperature in China as a whole (e.g., Jiang et al., 2003), what the LGM East Asian climate is seen in the coupled atmosphere–ocean general circulation models (AOGCMs) and whether results from AOGCMs are more consistent with proxy data than those of AGCMs in China remain unresolved questions. Fortunately, a number of simulations of the LGM climate using a hierarchy of models, ranging from AGCMs (either with prescribed SSTs or coupled with slab ocean models) to AOGCMs and the coupled atmosphere–ocean–vegetation general circulation models (AOVGCMs), are archived in the database of the PMIP. They provide a good opportunity for us to investigate the common responses of climate models to the presence of massive ice sheets and lower atmospheric CO_2 concentration during the LGM, and to

examine model-dependent uncertainties in China as well.

On the other hand, a great deal of reconstruction of the LGM climate in China has been undertaken through the use of ice cores, pollen, fluvial and marine data, lacustrine sediments, loesses, and so on. Regional climate was found to undergo dramatic changes during the LGM, with much colder than present surface temperature conditions. These proxy data form a solid foundation upon which model-data comparison can be made in a qualitative or quantitative manner. This begs the question as to the extent to which reconstructions and state-of-the-art simulations are compatible in mainland China. In an attempt to address the above issues, in this study the authors make use of 25 climate models' simulations within the PMIP to examine the LGM climate and then to perform a model-data comparison in China. It should be noted that, different from previous model-data comparisons based on individual AGCM's result (e.g., Chen et al., 2001; Liu et al., 2002; Jiang et al., 2003; Yu et al., 2003), the present comparison between multiple climate models and a wealth of proxy data is more helpful to uncover the ability of current climate models to reproduce the East Asian monsoon climate during the LGM, with respect to reconstructions. Moreover, of importance is that insights gained from this regional scale case study will contribute to a global perspective of model-data comparison during the LGM, as model-data comparison in China is absent in the scientific literature.

This article is organized as follows: section 2 introduces climate models' data, boundary conditions and experimental designs under the PMIP protocol for the LGM climate simulation, as well as a preliminary evaluation of the ability of models to reproduce the modern climatology in China; in section 3, the LGM climate conditions in China are examined, focusing mainly on the ensemble mean of climate models' results; section 4 performs a

model-data comparison; finally, conclusion is given in Section 5.

2. Data

The present study examines all of the simulations for the LGM climate under the framework of the PMIP, including experiments using nine AGCMs with prescribed sea surface temperatures (SSTs) established by CLIMAP (1981) (SST-f) and eight AGCMs with SSTs computed by slab ocean models (SST-c) in the first phase of the PMIP (PMIP1), and six AOGCMs and one AOVGCM in the second phase of the PMIP (PMIP2). In addition, a set of SST-f experiments carried out by an AGCM developed at the Institute of Atmospheric Physics under the Chinese Academy of Sciences (Jiang et al., 2003; hereinafter referred to as IAP) are also involved here. Basic information of these 25 models is listed in Table 1.

The boundary conditions for the LGM consist of changes in the Earth's orbital parameters (Berger, 1978), ice-sheet extent, and concentrations of atmospheric greenhouse gases. SSTs are prescribed as CLIMAP (1981) in the PMIP1 SST-f experiments, but computed by slab ocean models in the PMIP1 SST-c experiments and by oceanic general circulation models in the PMIP2 experiments. The ICE-4G and ICE-5G ice-sheet reconstructions are respectively used in the PMIP1 and PMIP2 experiments (Peltier, 1994, 2004). Atmospheric CO_2 concentration varies from 345 ppm for the control run to 200 ppm for the LGM simulation in the PMIP1 experiments (Raynaud et al., 1993), while concentrations of atmospheric CO_2, CH_4, and N_2O vary from pre-industrial values of 280 ppm, 760 ppb, and 270 ppb to 185 ppm, 350 ppb, and 200 ppb during the LGM in the PMIP2 experiments, respectively (Fluckiger et al., 1999; Dallenbach et al., 2000; Monnin et al., 2001). In addition, there are also differences in the

110 baseline (or reference) period for the LGM climate simulations. The modern period around 1950 is used in the PMIP1 SST-f experiments, and the pre-industrial period around 1750 is used 112 in the PMIP1 SST-c and PMIP2 experiments. More detail about boundary conditions and experimental designs of the LGM climate simulations can be found in Joussaume and Taylor 114 (1995), Braconnot et al. (2007), and at the website http://pmip.lsce.ipsl.fr/.

Since the extent to which climate models can reproduce the modern geographical 116 distribution and value of annual surface temperature and precipitation bears directly on whether their results are appropriate in addressing the LGM climate, spatial correlation coefficient (SCC) 118 between observation and control simulation and root mean square error excluding systematic model error (RMSE) of each control simulation, with respect to observation, are calculated on 120 the basis of 77 grid points in the Chinese mainland, respectively. The former (latter) variable is used to quantify similarity (internal model errors) between simulated and observed spatial 122 patterns. As is listed in Table 2, SCCs range from 0.77 (CCSR1) to 0.99 (UKMO, HadCM3M2, and HadCM3M2-veg), and RMSEs range from 1.19 (HadCM3M2) to 5.43^{o}C (CCSR1), 124 indicating that the models have a dependable ability to simulate the geographical distribution of annual surface temperature for the baseline period of 1979–2000 in China. Where the ensemble 126 mean, with the same weights, of the 25 models' results for annual surface temperature is concerned, SCC is 0.97, and RMSE is 2.06^{o}C.

128 There is a large spread for the ability of models to reproduce annual precipitation for the baseline period of 1979–2000 in China (Table 2). SCCs range from -0.12 (GEN1) to 0.93 130 (HadCM3M2), and RMSEs range from 0.66 (HadCM3M2) to 3.47 mm/day (LMD4). To identify "reliable" models for annual precipitation, three preconditions are arbitrarily set in the

present study. The first is SCC being positive and statistically significant at the 99% confidence level; the second is RMSE being smaller than 2 mm/day; and the last is the availability of evaporation data, as precipitation minus evaporation will be used to evaluate net precipitation (or moisture) conditions during the LGM. 15 models are finally chosen for analysis in terms of Table 2. For the ensemble mean, with the same weights, of the 15 models' results for annual precipitation in the baseline period, SCC is 0.87, and RMSE is 0.74 mm/day. Taken together, the multi-model ensemble mean has a higher reliability with reference to most, but not all, individual models as a whole, which justifies us in emphasizing the ensemble mean of the 25 (15) models' results for annual surface temperature (precipitation) in the following analysis.

3. LGM climate in China: results of PMIP simulations

3.1. Surface temperature

The LGM surface temperature differed greatly from that in the baseline period. In response to the LGM forcings, statistically significant annual surface temperature decreases of 2.0–7.0^{o}C were obtained from the ensemble mean of the 25 models' experiments (hereinafter referred to as MME-25) in the mainland of China (Figure 1a). On the whole, surface temperature reduction intensified towards high latitudes and was characterized by large magnitude over most parts of the Qinghai-Tibetan Plateau and over Northeast China, where annual surface cooling exceeded 5.0^{o}C. Taking the Chinese mainland as a whole, the MME-25 annual surface temperature decreased on average by 4.46^{o}C during the LGM with reference to baseline climate. As seen in Table 3, although the LGM regionally-averaged annual surface temperature in China reduced consistently in the 25 models' simulations, the magnitude of

surface cooling was different between the models, ranging from 1.49 (BMRC2) to 9.32°C (CCC2.0-slab), with a standard deviation of 1.68°C across the models. When viewed in terms of model classes, it was found that the geographical distribution of changes in the LGM annual surface temperature was similar between each other, but with different magnitude (Figure 1b–d). Annual surface cooling was the most strongest in the ensemble mean of the eight PMIP1 SST-c experiments (-5.63°C in China), whereas it was the most weakest in the ensemble mean of the 10 PMIP1 SST-f experiments (-3.44°C in China). Regionally-averaged annual surface temperature in China reduced by 4.59°C in the ensemble mean of the seven PMIP2 experiments. The less surface cooling in the PMIP1 SST-f experiments with prescribed SSTs (CLIMAP, 1981) can be, at least partly, attributed to small reduction in reconstructed SSTs in the adjacent oceans of East Asia. According to the availability of SSTs data, the simulated changes in the LGM SSTs as derived from the six PMIP2 AOGCMs' simulations were compared to that in CLIMAP (1981). In the western North Pacific (105–180°E and 0–40°N), for example, regionally-averaged annual SST during the LGM was 2.34°C (1.93°C in FGOALS, 1.96°C in CCSM, 2.03°C in MIROC3.2, 2.49°C in CNRM, 2.72°C in IPSL, and 2.92°C in HadCM3M2) colder than baseline climate in the AOGCMs' experiments, which was significantly stronger than 1.24°C in CLIMAP (1981). Accordingly, the LGM annual surface cooling in China was larger in the AOGCMs' experiments, as the corresponding colder SSTs in the western North Pacific can give rise to a larger (less) loss (gain) of surface heat in the East Asian region during boreal warm (winter) seasons.

The geographical distribution of LGM–baseline anomalies in seasonal surface temperature altered with season and was in general similar to the annual mean pattern described

above in East Asia, excluding over and around the seas off the east coast of the Asian continent within 118–128°E and 30–40°N. In this area, surface temperature changed by -10.0 to -14.0°C in winter (December, January, and February) and -3.0 to 1.0°C in summer (June, July, and August), which was directly associated with the reconstructed land environment there, rather than the modern ocean conditions, owing to a sea level lowering of about 120 meters during the LGM relative to the present day (Peltier, 1994, 2004). Where the whole Chinese mainland is concerned, the LGM surface cooling differed in magnitude between the seasons, ranging from -3.85°C in spring (March, April, and May), -4.21°C in summer, -4.60°C in winter, to -5.19°C in autumn (September, October, and November) in terms of the MME-25 (Table 3). Moreover, the LGM change in surface temperature, with respect to baseline climate, was largely different between the models in each season. It varied from 0.07 (BMRC2) to -9.37°C (CCC2.0-slab) in spring, -0.90 (IAP) to -10.26°C (CCC2.0-slab) in summer, -1.91 (BMRC2) to -10.71°C (CCM1) in autumn, and -1.55 (FGOALS) to -8.18°C (CCC2.0-slab) in winter, with the smallest (largest) standard deviation of 1.64°C (1.99°C) across the models in winter (summer). In addition, as with the annual mean, in each season the magnitude of surface temperature cooling was the most strongest in the ensemble mean of the eight PMIP1 SST-c experiments, with values of -5.08°C in spring, -5.29°C in summer, -6.77°C in autumn, and -5.39°C in winter, whereas it was the most weakest in the ensemble mean of the 10 PMIP1 SST-f experiments, with values of -2.78°C in spring, -3.03°C in summer, -3.92°C in autumn, and -4.03°C in winter. Surface temperature reduced by 3.98°C in spring, 4.67°C in summer, 5.21°C in autumn, and 4.49°C in winter in the ensemble mean of the seven PMIP2 experiments, respectively.

3.2. Precipitation

Annual precipitation reduced by 5–40% in China during the LGM, with respect to baseline climate, in terms of the ensemble mean of the 15 models' experiments (hereinafter referred to as MME-15) (Figure 2a). Statistically significant changes in annual precipitation were registered in northern Northeast China, northernmost Xinjiang, the central part of the Tibetan-Qinghai Plateau, and Southeast China, where annual precipitation reductions were 20–40% of the baseline values. The spatial pattern and magnitude of the LGM changes in annual precipitation were similar overall between each of the three types of experiments, although there were difference, mostly in magnitude, at the sub-regional scale (Figures 2b–d). Of significant difference was that annual precipitation increased slightly in the PMIP1 SST-c experiments but decreased in the rest two types of experiments in Southwest China. As listed in Table 4, at the national scale, regionally-averaged annual precipitation reduced by 20% (0.60 mm/day) in the MME-15 and was uniformly negative across the models, with a range of values from -6% (GFDL) to -38% (ECHAM3). On the whole, the LGM annual precipitation reduction was stronger in the ensemble mean of the six PMIP1 SST-f experiments (-27%) than those of the six PMIP1 SST-c experiments (-15%) and the three PMIP2 experiments (-17%).

The percentage change of seasonal precipitation during the LGM, relative to baseline climate, was similar, both in sign and spatial pattern, between the seasons and agreed in general with the annual mean case in much of China. By contrast, there were also differences, both in sign and magnitude, in some parts of China. In the MME-15, for example, the LGM precipitation increased by 0–10% over most parts of Southwest China in winter and 0–30% over the seas off the east coast of the East Asian continent around 125^{o}E and 35^{o}N in summer, whereas it decreased by more than 40% in the latter region in both winter and autumn. On the

other side, regionally-averaged precipitation in China was uniformly decreased across the seasons in the MME-15, with values of -16% in spring, -21% in summer, -26% in autumn, and -14% in winter. Changes in the LGM seasonal precipitation were the same in sign but different in magnitude among the three types of experiments (Table 4). The percentage anomaly of regionally-averaged seasonal precipitation was obviously stronger in the six PMIP1 SST-f simulations than it was in the rest nine PMIP1 SST-c and PMIP2 simulations. In addition, in each season, the LGM changes in regionally-averaged seasonal precipitation were greatly different between the models, with a wide range of values from -3% (GFDL) to -34% (ECHAM3) in spring, -6% (GFDL) to -33% (GEN2) in summer, -5% (UKMO) to -71% (ECHAM3) in autumn, and 10% (HadCM3M2) to -49% (BMRC2) in winter.

3.3. Evaporation

During the LGM, annual evaporation in China reduced by 5–40% in the MME-15, which was related directly to the LGM surface cooling. Statistically significant reduction in annual evaporation occurred mainly in East China and the central and western Qinghai-Tibetan Plateau, with negative anomalies of 15% to 40% (Figure 3a). The magnitude of change in annual evaporation during the LGM was similar, but its spatial pattern was somewhat different between each of the three types of experiments (Figures 3b–d). For example, the obtained large reduction of more than 30% in annual evaporation in the PMIP1 SST-f and SST-c experiments was not seen in the three PMIP2 experiments in Southeast China. The spatial variability of the LGM annual evaporation change was larger in the PMIP2 experiments than those in the remaining experiments, particularly in West China and North China, which was probably connected with the less number of climate models in the PMIP2 experiments. It can be found in

Table 4 that the LGM regionally-averaged annual evaporation in China decreased in all the PMIP experiments, ranging from -9% (GFDL) to -34% (ECHAM3). It reduced by an average of 21% (0.41 mm/day) in the MME-15. Moreover, the magnitude of the LGM change in regionally-averaged annual evaporation was comparable between each of the three types of experiments, with values of -24% in the PMIP1 SST-f simulations, -19% in the PMIP1 SST-c simulations, and -21% in the PMIP2 simulations.

Seasonal evaporation during the LGM reduced overall in the Chinese mainland, with a similar magnitude to the annual mean on a large scale. At the sub-regional scale, however, the percentage change in the LGM seasonal evaporation differed with the seasons, particularly over and around the region of 118–128^{o}E and 30–40^{o}N. In this area, the LGM evaporation reduced by more than 40% in winter and autumn but increased by more than 40% in summer, which was related directly to the LGM surface temperature anomalies described above and can be attributed to the assigned change in surface boundary condition from the modern seas to the reconstructed land during the LGM (Peltier, 1994, 2004). As given in Table 4, the LGM regionally-averaged seasonal evaporation in China reduced by 20% in spring, 15% in summer, 27% in autumn, and 36% in winter on the basis of the MME-15. Its change was uniformly negative across the 15 models, with a wide range of values from -8% (GFDL) to -46% (CCC2.0-slab) in spring, -3% (GFDL) to -26% (CCC2.0-slab) in summer, -14% (GFDL and UKMO) to -50% (ECHAM3) in autumn, and -19% (MRI2) to -56% (BMRC2) in winter. Moreover, in each season, percentage change in the LGM evaporation was comparable in magnitude between each of the three types of experiments and was near the average value as derived from the MME-15.

4. Model-data comparison

Using a variety of proxy records, considerable effort has been made by scientists to reconstruct climate conditions in China during the LGM. To the knowledge of the authors, the LGM surface temperature reconstructions that have been expressed in a quantitative manner are given in Table 5. According to the spatial coverage of proxy data, four regions covering most parts of the Chinese mainland are selected in this study to perform a model-data comparison. As seen in Table 6, proxy estimates of annual surface temperature change during the LGM were uniformly negative compared to the present day, with values of -7.0 $\pm$3.5^{o}C in South China, -6 to -9^{o}C in the Qinghai-Tibetan Plateau, -13 to -15^{o}C in Hexi Corridor, and at least -8 to -10^{o}C in North and Northeast China. On the whole, the PMIP models reproduce successfully surface cooling trend during the LGM, but fail to reproduce its magnitude in these regions, particularly in the latter two regions. In the MME-25, regionally-averaged annual surface temperature during the LGM reduced by 3.39^{o}C in South China, 5.05^{o}C in the Qinghai-Tibetan Plateau, 4.68^{o}C in Hexi Corridor, and 4.86^{o}C in North and Northeast China, respectively, all of which were smaller than the reconstructed values. If inter-model variability, represented by the standard deviation of model results about the mean, of simulated surface temperature change is taken into account, the MME-25 lies in the low range of proxy estimates in South China and the Qinghai-Tibetan Plateau. However, model-data discrepancy in magnitude is still substantial and cannot be reconciled in the remaining two regions.

As with the case of the whole Chinese mainland, the magnitude of annual surface temperature changes during the LGM differs between the model classes, with the largest (smallest) being in the 10 (eight) PMIP1 SST-c (SST-f) experiments in all the four regions

(Table 6). The results of the seven PMIP2 experiments lie in the range between the PMIP1 SST-c and SST-f experiments. Meanwhile, model spread is also the largest in the PMIP1 SST-c experiments in the four regions where the standard deviation of model results varies from 1.57 to 3.47^{o}C depending on the region. In general, the PMIP1 SST-c (SST-f) experiments are in the best (poorest) agreement with proxy estimates of surface temperature among the PMIP experiments, and the PMIP experiments with computed SSTs are in better agreement with proxy estimates than those with prescribed SSTs. That means that interactive ocean plays an important role in forming climate conditions in China during the LGM.

On the other side, a reconstruction of annual water budget used in the present model-data comparison is described in Yu et al. (2003) and references therein, in which a number of lake status records have revealed that LGM climate conditions were drier in eastern China but somewhat wetter in western China than at the present day (Figure 4). Unlike most previous studies comparing simulated precipitation changes directly with dry or wet conditions estimated by proxy data (e.g., Pinot et al., 1999; Kageyama et al., 2001; Jiang et al., 2003; Hoar et al., 2004; Braconnot et al., 2007), simulated LGM–baseline (or LGM-minus-baseline) anomalies in precipitation minus evaporation (P–E, an appropriate variable to represent moisture conditions) were used in this study. In terms of the MME-15, annual P–E decreased by 0.00–0.60 mm/day in the Chinese mainland excluding part of western China (about 74–97^{o}E and 35–42^{o}N) and southeastern Sichuan Province (about 105^{o}E and 28^{o}N) where annual P–E increased by less than 0.10 mm/day (Figure 4a). At the national scale, regionally-averaged annual P–E during the LGM decreased by 18% (0.19 mm/day) in China relative to a baseline annual P–E value of 1.07 mm/day. LGM–baseline anomalies in annual P–E differed between

the models, particularly a positive value (0.16 mm/day) being obtained by CCC2.0-slab, and between each of the three types of experiments, with values of -33% (-0.31 mm/day) from the six PMIP1 SST-f models, -9% (-0.10 mm/day) from the six PMIP1 SST-c models, and -12% (-0.13 mm/day) from the three PMIP2 models. In addition, seasonal mean P–E during the LGM increased by 39% (0.15 mm/day) in winter, but decreased by 10% (0.12 mm/day) in spring, 30% (0.62 mm/day) in summer, and 24% (0.16 mm/day) in autumn. As such, annual P–E reduction during the LGM was mainly derived from more reduction in seasonal mean P–E in summer, which was due directly to a systematic weakening of the East Asian summer monsoon during the LGM with respect to baseline climate (Jiang and Lang, 2010, manuscript submitted to *Journal of Climate*).

Model-data comparison indicates that large-scale LGM–baseline anomalies in annual P–E in the MME-15 agree well with the lake status-based reconstruction of changes in annual water balance in most parts of the Chinese mainland (Figure 4a). Among these include drier conditions in East China about east of 100^{o}E and wetter conditions in the region of about 74–97^{o}E and 35–42^{o}N. By contrast, model-data disagreement occurs in the Qinghai-Tibetan Plateau and part of the northern Uygur Autonomous Region of Xinjiang, where simulated drier conditions were opposite in sign to the wetter conditions estimated by reconstructed higher lake levels and fresher water than the modern period during the LGM (Yu et al., 2003). However, it is worth noting that, contrary to the wetter conditions derived from lake status records, pollen data from seven sampling sites covering the eastern Qinghai-Tibetan Plateau (92–102^{o}E, 30–37^{o}N) suggested a much drier climate conditions during the LGM (Tang et al., 1998), in line with the MME-15. Taken together, it is not possible at the moment to evaluate whether the

MME-15 is compatible with reconstructions in this area until a common result is obtained from a variety of proxy data. In the Qinghai-Tibetan Plateau, the LGM annual precipitation reduced by 15–40% in the MME-15 (Figure 2a), which supports a 30–70% reduction in annual precipitation deduced by Shi et al. (1997).

In addition, Figures 4b–d show that, although there are differences both in the spatial pattern and magnitude of changes in annual P–E during the LGM between each of the three types of PMIP experiments, drier-than-modern conditions occur overall in East China about east of 100^{o}E and the Qinghai-Tibetan Plateau across these experiments. Apparent disagreement between the model classes appears in West China excluding the Qinghai-Tibetan Plateau, in which region drier condition is obtained by the six PMIP1 SST-f models, whereas opposite situation is derived from the six PMIP1 SST-c models and three PMIP2 models. In this regard, the PMIP simulations with computed (fixed) SSTs are consistent (inconsistent) with proxy data in these regions during the LGM. Additionally, it should be noted that, in the Qinghai-Tibetan Plateau, annual P–E was found to keep constant or increase by around 0.50 mm/day in an AGCM experiment, which was then used to explain wetter conditions during the LGM (Yu et al., 2001). Based on the present study, this cause-and-effect relationship is obviously model-dependent, as annual P–E during the LGM reduced uniformly in the ensemble mean of the PMIP simulations either with prescribed or computed SSTs (Figure 4).

5. Conclusion

In this study, climate conditions in the Chinese mainland during the LGM are investigated on the basis of the results of PMIP simulations from 10 AGCMs with prescribed SSTs, eight

AGCMs coupled with slab ocean models, six AOGCMs, and one AOVGCM. The primary conclusions are as follows:

(1) All the 25 models reproduced a cold-than-baseline climate in China during the LGM, and regionally-averaged annual surface temperature reduced by 4.46^{o}C, ranging from 1.49 to 9.32^{o}C depending on the model. Surface cooling was greater in the simulations with computed SSTs than those with prescribed SSTs, and the less in the latter can be, at least partly, attributed to a systematic weakness of reconstructed changes in SSTs (CLIMAP, 1981) in the adjacent oceans of East Asia.

(2) During this period, both annual precipitation and evaporation in China reduced across the simulations from all the 15 models chosen for analysis. More of the reduction of precipitation than that of evaporation gave rise to a drier-than-baseline climate in much of China during the LGM. At the national scale, the LGM annual P–E reduced by 18% (0.19 mm/day) compared to baseline climate.

(3) The 25 models in general underestimate the magnitude of surface cooling during the LGM, as suggested by proxy data, in the four regions of China where model-data comparison is performed. The simulations with computed SSTs are in better agreement with proxy estimates of surface temperature than those with prescribed SSTs. On the other hand, the 15-model simulated large-scale LGM–baseline anomalies in annual P–E agree qualitatively well with lake status-based reconstruction of changes in annual water budget in East and part of West China.

Taken together, the first lesson learned from the present study is that the ocean is an important component of the climate system in the East Asian monsoon area during the LGM, as

372 the simulations with interactive ocean are in better agreement with proxy estimates in the Chinese mainland than the PMIP1 SST-f simulations. In this regard, the response of the ocean
374 to the LGM forcings needs to be accounted for using the PMIP2 simulations to understand the role of the ocean feedback on the East Asian climate during the LGM. In addition, simulated
376 annual surface temperature during the LGM was lower in the PMIP1 SST-c simulations than the PMIP2 simulations in all the regions of model-data comparison, with an additional cooling
378 of 1.25^{o}C in South China, 1.49^{o}C in the Qinghai-Tibetan Plateau, 0.76^{o}C in Hexi Corridor, and 1.15^{o}C in North and Northeast China (Table 6). This raises the question as to the reason why
380 AGCMs coupled with simple slab ocean models tend to do a better job, with reference to proxy evidence. It is a pity that SSTs from the PMIP1 SST-c simulations are not available in the PMIP
382 database, which makes it impossible for the authors to perform a preliminary investigation.

Vegetation feedback has been proposed as an important potential process contributing to
384 the LGM climate (e.g., Crowley and Baum, 1997; Levis et al., 1999; Crucifix and Hewitt, 2005; Jansen et al., 2007). Using AGCMs with reconstructed vegetation or coupled with vegetation
386 model, earlier simulations of the LGM climate have shown that changes in vegetation can induce additional climate change, which in general reduces model-data disagreement in surface
388 temperature in the Chinese mainland (Chen et al., 2001; Yu et al., 2001; Jiang et al., 2003; Jiang, 2008). The PMIP2 simulations using HadCM3M2 and HadCM3M2-veg provide an
390 opportunity to evaluate the effect of vegetation on the East Asian climate in the fully coupled climate model during the LGM, as dynamical vegetation model is the main difference between
392 the two models (Michel Crucifix, personal communication, 2009). As seen in Table 3, annual surface temperature during the LGM was 2.00^{o}C colder in HadCM3M2-veg (-6.61^{o}C) than its

AOGCM counterpart (-4.61^{o}C), and seasonal surface temperature was also much colder in the former than it was in the latter. Accordingly, the results of surface temperature obtained in HadCM3M2-veg are more consistent with proxy estimates in China, particularly in South China and the Qinghai-Tibetan Plateau where this simulation agrees well with proxy records (Table 6). In this connection, the vegetation is another important component in determining the East Asian climate during the LGM, although the underlying mechanism needs to be further explored.

Besides the models themselves, another source, at least partly, responsible for model-data mismatch is uncertainty in the proxy data. This is especially true in the eastern Qinghai-Tibetan Plateau, where wetter conditions derived from lake status records during the LGM (Yu et al., 2003) was opposite to drier conditions derived from pollen records (Tang et al., 1998). Given that the spatial coverage of proxy data used for the present model-data comparison is rather sparse, more reconstruction work using a variety of proxy data and ways is urgently needed to test model results and, hence, to improve our knowledge of the LGM climate in the East Asian monsoon area.

Acknowledgements. We acknowledge the international modeling groups for providing their data for analysis, the Laboratoire des Sciences du Climat et de l'Environnement (LSCE) for collecting and archiving the model data. This research is supported by the Chinese National Basic Research Program of China (Grant No. 2009CB421407) and National Natural Science Foundation (Grant Nos. 40775052 and 40975050). The PMIP2/MOTIF Data Archive is supported by CEA, CNRS, the EU project MOTIF (EVK2-CT-2002-00153) and the Programme National d'Etude de la Dynamique du Climat (PNEDC). The analyses were performed using version 27 December 2008 of the database. More information is available on http://pmip2.lsce.ipsl.fr/ and http://motif.lsce.ipsl.fr/.

418 ## References

Berger, A., 1978: Long-term variations of daily insolation and Quaternary climatic changes. 420 *Journal of the Atmospheric Sciences*, **35**, 2362–2367.

Braconnot, P., and Coauthors, 2007: Results of PMIP2 coupled simulations of the 422 Mid-Holocene and Last Glacial Maximum – Part 1: experiments and large-scale features. *Climate of the Past*, **3**, 261–277.

424 Chen, X., G. Yu, and J. Liu, 2001: An AGCM+SSiB model simulation on changes in palaeomonsoon climate at 21 ka BP in China. *Acta Meteorologica Sinica*, **15**, 333–345.

426 CLIMAP project members, 1981: Seasonal reconstructions of the Earth's surface at the Last Glacial Maximum. *Map Chart Ser. MC-36*, Geol. Soc. of Am., Boulder, Colorado.

428 Crowley, T. J., and S. K. Baum, 1997: Effect of vegetation on an ice-age climate model simulation. *Journal of Geophysical Research*, **102**(D14), 16463–16480.

430 Crucifix, M., and C. D. Hewitt, 2005: Impact of vegetation changes on the dynamics of the atmosphere at the Last Glacial Maximum. *Climate Dynamics*, **25**, 447–459.

432 Dallenbach, A., T. Blunier, J. Fluckiger, B. Stauffer, J. Chappellaz, and D. Raynaud, 2000: Changes in the atmospheric CH_4 gradient between Greenland and Antarctica during the 434 Last Glacial and the transition to the Holocene. *Geophysical Research Letters*, **27**, 1005–1008.

436 Farrera, I., and Coauthors, 1999: Tropical climates at the Last Glacial Maximum: a new synthesis of terrestrial palaeoclimate data. I. Vegetation, lake-levels and geochemistry. 438 *Climate Dynamics*, **15**, 823–856.

Fluckiger, J., A. Dallenbach, T. Blunier, B. Stauffer, T. F. Stocker, D. Raynaud, and J. M. 440 Barnola, 1999: Variations in atmospheric N_2O concentration during abrupt climatic

changes. *Science*, **285**, 227–230.

Herzschuh, U., H. Kürschner, and S. Mischke, 2006: Temperature variability and vertical vegetation belt shifts during the last ~50,000 yr in the Qilian Mountains (NE margin of the Tibetan Plateau, China). *Quaternary Research*, **66**, 133–146.

Hoar, M. R., J. P. Palutikof, and M. C. Thorne, 2004: Model intercomparison for the present day, the mid-Holocene, and the Last Glacial Maximum over western Europe. *Journal of Geophysical Research*, **109**, D08104, doi:10.1029/2003JD004161.

Jansen, E., and Coauthors, 2007: Palaeoclimate. In: *Climate Change 2007: The Physical Science Basis. Contribution of Working Group I to the Fourth Assessment Report of the Intergovernmental Panel on Climate Change* [Solomon, S., D. Qin, M. Manning, Z. Chen, M. Marquis, K.B. Averyt, M. Tignor, and H. L. Miller (Eds.)]. Cambridge University Press, Cambridge, United Kingdom and New York, NY, USA, pp. 434–497.

Jiang, D., 2008: Vegetation and soil feedbacks at the Last Glacial Maximum. *Palaeogeography, Palaeoclimatology, Palaeoecology*, **268**, 39–46.

Jiang, D., H. J. Wang, H. Drange, and X. Lang, 2003: Last Glacial Maximum over China: Sensitivities of climate to paleovegetation and Tibetan ice sheet. *Journal of Geophysical Research*, **108**(D3), 4102, doi: 10.1029/2002JD002167.

Joussaume, S., and K. E. Taylor, 1995: Status of the Paleoclimate Modeling Intercomparison Project (PMIP), In: *Proceedings of the First International AMIP Scientific Conference, WCRP-92, WMO/TD-732* [Gates, W. L. (Eds.)]. World Meteorological Organization, Geneva, pp. 425–430.

Ju, L. X., H. J. Wang, and D. Jiang, 2007: Simulation of the Last Glacial Maximum climate over East Asia with a regional climate model nested in a general circulation model.

464 *Palaeogeography, Palaeoclimatology, Palaeoecology*, **248**, 376–390.

Kageyama, M., O. Peyron, S. Pinot, P. Tarasov, J. Guiot, S. Joussaume, and G. Ramstein, 2001:
466 The last glacial maximum over Europe and western Siberia: a PMIP comparison between models and data. *Climate Dynamics*, **17**, 23–43.

468 Kageyama, M., and Coauthors, 2006: Last Glacial Maximum temperatures over the North Atlantic, Europe and western Siberia: a comparison between PMIP models, MARGO
470 sea-surface temperatures and pollen-based reconstructions. *Quaternary Science Reviews*, **25**, 2082–2102.

472 Kalnay, E., and Coauthors, 1996: The NCEP/NCAR Reanalysis Project. *Bulletin of the American Meteorological Society*, **77**, 437–472.

474 Levis, S., J. A. Foley, and D. Pollard, 1999: CO_2, climate, and vegetation feedbacks at the Last Glacial Maximum. *Journal of Geophysical Research*, **104**(D24), 31191–31198.

476 Liu, J., G. Yu, and X. Chen, 2002: Palaeoclimate simulation of 21 ka for the Tibetan Plateau and Eastern Asia. *Climate Dynamics*, **19**, 575–583.

478 Liu, K.-B., 1988: Quaternary history of the temperate forests of China. *Quaternary Science Reviews*, **7**, 1–20.

480 Liu, X., X. Wu, G. Dong, B. Dong, and P. J. Valdes, 1995: A modeling research on East Asia monsoonal climate at the Last Glacial Maximum (in Chinese). *Scientia Meteorologica*
482 *Sinica*, **15**, 183–196.

Lu, H.-Y., N.-Q. Wu, K.-B. Liu, H. Jiang, and T.-S. Liu, 2007: Phytoliths as quantitative
484 indicators for the reconstruction of past environmental conditions in China II: palaeoenvironmental reconstruction in the Loess Plateau. *Quaternary Science Reviews*,
486 **26**, 759–772.

Masson-Delmotte, V., and Coauthors, 2006: Past and future polar amplification of climate change: climate model intercomparisons and ice-core constraints. *Climate Dynamics*, **26**, 513–529.

Monnin, E., A. Indermuhle, A. Dallenbach, J. Fluckiger, B. Stauffer, T. F. Stocker, D. Raynaud, and J. M. Barnola, 2001: Atmospheric CO_2 concentrations over the last glacial termination. *Science*, **291**, 112–114.

Otto-Bliesner, B. L., and Coauthors, 2009: A comparison of PMIP2 model simulations and the MARGO proxy reconstruction for tropical sea surface temperatures at last glacial maximum. *Climate Dynamics*, **32**, 799–815.

Peltier, W. R., 1994: Ice age paleotopography. *Science*, **265**, 195–201.

Peltier, W. R., 2004: Global glacial isostasy and the surface of the ice-age earth: the ICE-5G (VM2) model and GRACE. *Annual Review of Earth and Planetary Sciences*, **32**, 111–149.

Pinot, S., G. Ramstein, S. P. Harrison, I. C. Prentice, J. Guiot, M. Stute, and S. Joussaume, 1999: Tropical paleoclimates at the Last Glacial Maximum: comparison of Paleoclimate Modeling Intercomparison Project (PMIP) simulations and paleodata. *Climate Dynamics*, **15**, 857–874.

Ramstein, G., M. Kageyama, J. Guiot, H. Wu, C. Hély, G. Krinner, and S. Brewer, 2007: How cold was Europe at the Last Glacial Maximum? A synthesis of the progress achieved since the first PMIP model-data comparison. *Climate of the Past*, **3**, 331–339.

Raynaud, D., J. Jouzel, J. M. Barnola, J. Chappellaz, R. J. Delmas, and C. Lorius, 1993: The ice record of greenhouse gases. *Science*, **259**, 926–934.

Shi, Y., 2002: Characteristics of late Quaternary monsoonal glaciation on the Tibetan Plateau

and in East Asia. *Quaternary International*, **97–98**, 79–91.

Shi, Y., B. Zheng, and T. Yao, 1997: Glaciers and environments during the Last Glacial Maximum (LGM) on the Tibetan Plateau (in Chinese). *Journal of Glaciology and Geocryology*, **19**, 97–113.

Su, Z., and Y. Ma, 1997: The discovery of palaeo-eolian formed in the last glacial maximum and environmental evolution in the Northwest of Shanxi (in Chinese). *Journal of Desert Research*, **17**, 389–394.

Tang, L.-Y., C.-M. Shen, Z.-Z. Kong, F.-B. Wang, and K.-B. Liu, 1998: Pollen evidence of climate during the Last Glacial Maximum in eastern Tibetan Plateau (in Chinese). *Journal of Glaciology and Geocryology*, **20**, 133–140.

Wang, H. J., and Q. C. Zeng, 1993: The numerical simulation of the ice age climate. *Acta Meteorologica Sinica*, **7**, 423–430.

Wang, N.-A., T. Wang, Z.-T. Shi, G. Hu, and S.-W. Gao, 2001: The discovery of sand wedges of the last glaciation in the Hexi Corridor and its paleoclimatic significance (in Chinese). *Journal of Glaciology and Geocryology*, **23**, 46–50.

Wang, Y. J., X. G. Kong, X. H. Shao, and J. Y. Wu, 2002: Century-scale climatic oscillations during the last glacial maximum recorded in a stalagmite from Nanjing (in Chinese). *Quaternary Sciences*, **22**, 243–251.

Wu N. Q., H. Y. Lü, X. J. Sun, Z. T. Guo, J. Q. Liu, and J. M. Han, 1994: Climate transfer function from opal phytolith and its application in paleoclimate reconstruction of China loess-paleosol sequence (in Chinese). *Quaternary Sciences*, **14**, 270–279.

Xie, P., and P. A. Arkin, 1997: Global precipitation: A 17-year monthly analysis based on gauge observations, satellite estimates, and numerical model outputs. *Bulletin of the*

American Meteorological Society, **78**, 2539–2558.

Yao, T., X. Liu, N. Wang, and Y. Shi, 2000: Amplitude of climatic changes in Qinghai-Tibetan Plateau. *Chinese Science Bulletin*, **45**, 1236–1243.

Yu, G., X. Chen, J. Liu, and S. Wang, 2001: Preliminary study on LGM climate simulation and the diagnosis for East Asia. *Chinese Science Bulletin*, **46**, 364–368.

Yu, G., B. Xue, J. Liu, and X. Chen, 2003: LGM lake records from China and an analysis of climate dynamics using a modelling approach. *Global and Planetary Change*, **38**, 223–256.

Zhang, B. Z., P. X. Zhang, T. K. Lowenstein, and R. J. Spencer, 1995: Time range of the great ice age of the last glacial stage and its related geological event of playa in the Qinghai-Xizang (Tibet) Plateau (in Chinese). *Quaternary Sciences*, **15**, 193–201.

Zhao, P., L. X. Chen, X. J. Zhou, Y. F. Gong, and Y. Han, 2003: Modeling the East Asian climate during the last glacial maximum. *Science in China (Series D)*, **46**, 1060–1068.

Zheng, Y. Q., G. Yu, S. M. Wang, B. Xue, D. Q. Zhuo, X. M. Zeng, and H. Q. Liu, 2004: Simulation of paleoclimate over East Asia at 6 ka BP and 21 ka BP by a regional climate model. *Climate Dynamics*, **23**, 513–529.

Zheng, Z., and J. Guiot, 1999: A 400000-year paleoclimate reconstruction in tropical region of China (in Chinese). *Acta Scientiarum Naturalium Universitatis Sunyaseni*, **38**, 94–98.

Tables:

552 Table 1. Basic information of general circulation models used in the present study

Model ID		Project	Atmospheric resolution (longitude x latitude, level)	Length of run analyzed (year)	Baseline period
01	BMRC2	PMIP1 (SST-f)	96 x 80, L17	15	Modern
02	CCC2.0	PMIP1 (SST-f)	96 x 48, L10	10	Modern
03	CCSR1	PMIP1 (SST-f)	64 x 32, L20	10	Modern
04	ECHAM3	PMIP1 (SST-f)	128 x 64, L19	10	Modern
05	GEN2	PMIP1 (SST-f)	96 x 48, L18	10	Modern
06	IAP	PMIP1 (SST-f)	72 x 46, L9	10	Modern
07	LMD4	PMIP1 (SST-f)	48 x 36, L11	15	Modern
08	LMD5	PMIP1 (SST-f)	64 x 50, L11	15	Modern
09	MRI2	PMIP1 (SST-f)	72 x 46, L15	10	Modern
10	UGAMP	PMIP1 (SST-f)	128 x 64, L19	20	Modern
11	CCC2.0-slab	PMIP1 (SST-c)	96 x 48, L10	10	Pre-industrial
12	CCM1	PMIP1 (SST-c)	48 x 40, L12	10	Pre-industrial
13	GEN1	PMIP1 (SST-c)	48 x 40, L12	14	Pre-industrial
14	GEN2-slab	PMIP1 (SST-c)	96 x 48, L18	10	Pre-industrial
15	GFDL	PMIP1 (SST-c)	96 x 80, L20	25	Pre-industrial
16	MRI2-slab	PMIP1 (SST-c)	72 x 46, L15	14	Pre-industrial
17	UGAMP-slab	PMIP1 (SST-c)	128 x 64, L19	20	Pre-industrial
18	UKMO	PMIP1 (SST-c)	96 x 73, L19	20	Pre-industrial
19	CCSM	PMIP2 (AOGCM)	128 x 64, L18	100	Pre-industrial
20	CNRM	PMIP2 (AOGCM)	128 x 64, L31	100	Pre-industrial
21	FGOALS	PMIP2 (AOGCM)	128 x 60, L9	100	Pre-industrial
22	HadCM3M2	PMIP2 (AOGCM)	96 x 73, L19	100	Pre-industrial
23	IPSL	PMIP2 (AOGCM)	96 x 72, L19	100	Pre-industrial
24	MIROC3.2	PMIP2 (AOGCM)	128 x 64, L20	100	Pre-industrial
25	HadCM3M2-veg	PMIP2 (AOVGCM)	96 x 73, L19	100	Pre-industrial

Table 2. Spatial correlation coefficient (SCC) and root mean square error excluding systematic model error (RMSE) of annual surface temperature and precipitation between each baseline (or control) simulation and observation on the basis of 77 grid points within mainland China*

Model ID		Annual surface temperature		Annual precipitation		
		SCC	RMSE (^{o}C)	SCC	RMSE (mm/day)	Analyzed or not
01	BMRC2	0.95	2.64	0.75	0.92	Yes
02	CCC2.0	0.88	3.95	0.52	1.51	Yes
03	CCSR1	0.77	5.43	0.79	0.81	Yes
04	ECHAM3	0.96	2.25	0.83	0.81	Yes
05	GEN2	0.95	2.52	0.82	1.06	Yes
06	**IAP**	0.89	3.60	0.69	1.16	No
07	LMD4	0.95	2.69	0.41	**3.47**	No
08	LMD5	0.97	2.52	0.66	**2.24**	No
09	MRI2	0.82	4.71	0.55	1.81	Yes
10	UGAMP	0.97	2.80	0.64	**2.13**	No
11	CCC2.0-slab	0.88	3.82	0.52	1.46	Yes
12	CCM1	0.78	5.22	0.79	1.09	Yes
13	GEN1	0.84	4.67	**-0.12**	1.41	No
14	GEN2-slab	0.95	2.56	0.84	1.17	Yes
15	GFDL	0.94	2.76	0.83	1.32	Yes
16	MRI2-slab	0.86	4.32	0.61	1.51	Yes
17	UGAMP-slab	0.97	2.67	0.64	**2.17**	No
18	UKMO	0.99	1.37	0.86	0.71	Yes
19	**CCSM**	0.94	2.80	0.69	0.96	No
20	CNRM	0.98	1.73	0.74	1.64	Yes
21	FGOALS	0.98	1.62	**0.27**	1.97	No
22	HadCM3M2	0.99	1.19	0.93	0.66	Yes
23	**IPSL**	0.96	2.51	0.60	1.08	No
24	**MIROC3.2**	0.95	2.75	0.79	0.86	No
25	HadCM3M2-veg	0.99	1.36	0.92	0.67	Yes

*Observational climatology is respectively derived from the NCEP/NCAR reanalysis of surface temperature (Kalnay et al., 1996) and the CPC merged analysis of precipitation (Xie and Arkin, 1997) for the period of 1979–2000. For annual precipitation, SCC with the confidence level below 99% is in bold; RMSE above 2 mm/day is in bold; and the model-ID whose evaporation data is not available is in bold.

560 Table 3. LGM–baseline anomalies in regionally-averaged annual surface temperature (units: ^{o}C) in China*

Model ID		Annual mean	Winter	Spring	Summer	Autumn
01	BMRC2	-1.49	-1.62	0.07	-2.49	-1.91
02	CCC2.0	-5.51	-3.69	-6.27	-6.65	-5.43
03	CCSR1	-3.26	-3.56	-3.03	-3.77	-2.69
04	ECHAM3	-2.77	-2.32	-1.24	-3.75	-3.78
05	GEN2	-3.96	-5.96	-2.56	-2.18	-5.13
06	IAP	-2.39	-3.94	-1.40	-0.90	-3.33
07	LMD4	-4.01	-5.92	-2.30	-2.37	-5.45
08	LMD5	-4.48	-5.95	-4.12	-3.06	-4.79
09	MRI2	-3.08	-3.47	-3.60	-1.86	-3.38
10	UGAMP	-3.47	-3.85	-3.38	-3.30	-3.35
11	CCC2.0-slab	-9.32	-8.18	-9.37	-10.26	-9.47
12	CCM1	-8.02	-7.70	-6.87	-6.78	-10.71
13	GEN1	-5.86	-5.74	-5.60	-5.15	-6.96
14	GEN2-slab	-3.48	-4.84	-2.41	-2.08	-4.59
15	GFDL	-4.25	-3.65	-3.45	-4.38	-5.50
16	MRI2-slab	-6.04	-5.01	-5.83	-6.06	-7.27
17	UGAMP-slab	-3.74	-3.51	-3.21	-3.78	-4.46
18	UKMO	-4.35	-4.54	-3.87	-3.82	-5.18
19	CCSM	-3.77	-3.97	-3.51	-3.55	-4.06
20	CNRM	-4.07	-5.19	-3.02	-3.40	-4.65
21	FGOALS	-3.65	-1.55	-3.61	-4.50	-4.93
22	HadCM3M2	-4.61	-4.90	-3.94	-4.55	-5.04
23	IPSL	-5.33	-4.66	-4.55	-5.93	-6.19
24	MIROC3.2	-4.07	-3.96	-3.38	-4.03	-4.92
25	HadCM3M2-veg	-6.61	-7.20	-5.82	-6.74	-6.67
MME-all		-4.46	-4.60	-3.85	-4.21	-5.19
MME-PMIP1-SST-f		-3.44	-4.03	-2.78	-3.03	-3.92
MME-PMIP1-SST-c		-5.63	-5.39	-5.08	-5.29	-6.77
MME-PMIP2		-4.59	-4.49	-3.98	-4.67	-5.21

562 *MME-all denotes the ensemble mean of the 25 models' results; MME-PMIP1-SST-f denotes the ensemble mean of the 10 PMIP1 SST-f models' results; MME-PMIP1-SST-c denotes the ensemble mean of the eight
564 PMIP1 SST-c models' results; and MME-PMIP2 denotes the ensemble mean of the seven PMIP2 models' results.

566 Table 4. Percentage anomaly (units: %) and difference (units: mm/day, expressed in parentheses) of regionally-averaged annual and seasonal precipitation and evaporation in China during the LGM with respect to baseline climate*

Model ID		Precipitation / Evaporation				
		Annual	Winter	Spring	Summer	Autumn
01	BMRC2	-25 (-0.67) / -29 (-0.51)	-49 (-0.45) / -56 (-0.37)	-25 (-0.72) / -25 (-0.50)	-10 (-0.47) / -18 (-0.49)	-47 (-1.03) / -43 (-0.67)
02	CCC2.0	-21 (-0.62) / -26 (-0.51)	8 (0.11) / -32 (-0.21)	-9 (-0.28) / -32 (-0.58)	-31 (-1.52) / -22 (-0.79)	-34 (-0.80) / -24 (-0.45)
03	CCSR1	-22 (-0.66) / -19 (-0.41)	1 (0.01) / -27 (-0.28)	-18 (-0.55) / -16 (-0.37)	-20 (-1.11) / -13 (-0.47)	-40 (-0.98) / -26 (-0.53)
04	ECHAM3	-38 (-0.77) / -34 (-0.49)	-43 (-0.27) / -53 (-0.37)	-34 (-0.65) / -34 (-0.48)	-24 (-0.90) / -18 (-0.41)	-71 (-1.25) / -50 (-0.71)
05	GEN2	-36 (-0.96) / -25 (-0.42)	-36 (-0.41) / -48 (-0.47)	-28 (-0.78) / -14 (-0.24)	-33 (-1.47) / -15 (-0.39)	-51 (-1.17) / -37 (-0.59)
09	MRI2	-24 (-1.05) / -18 (-0.53)	-26 (-0.48) / -19 (-0.25)	-18 (-0.92) / -16 (-0.50)	-29 (-1.99) / -18 (-0.83)	-22 (-0.81) / -21 (-0.54)
11	CCC2.0-slab	-17 (-0.48) / -32 (-0.64)	-3 (-0.05) / -48 (-0.34)	-22 (-0.67) / -46 (-0.87)	-20 (-1.00) / -26 (-0.92)	-9 (-0.20) / -22 (-0.42)
12	CCM1	-22 (-0.91) / -24 (-0.56)	-20 (-0.39) / -50 (-0.41)	-16 (-0.54) / -23 (-0.48)	-27 (-2.06) / -16 (-0.70)	-17 (-0.63) / -33 (-0.64)
14	GEN2-slab	-20 (-0.54) / -18 (-0.30)	-22 (-0.26) / -46 (-0.44)	-12 (-0.33) / -9 (-0.14)	-20 (-0.87) / -8 (-0.18)	-28 (-0.70) / -27 (-0.44)
15	GFDL	-6 (-0.20) / -9 (-0.16)	2 (0.03) / -22 (-0.16)	-3 (-0.13) / -8 (-0.19)	-6 (-0.32) / -3 (-0.10)	-16 (-0.39) / -14 (-0.21)
16	MRI2-slab	-13 (-0.49) / -16 (-0.41)	-8 (-0.13) / -25 (-0.32)	-13 (-0.55) / -17 (-0.45)	-17 (-0.98) / -11 (-0.42)	-8 (-0.29) / -19 (-0.46)
18	UKMO	-11 (-0.26) / -11 (-0.20)	-15 (-0.18) / -21 (-0.20)	-15 (-0.43) / -11 (-0.23)	-9 (-0.35) / -5 (-0.12)	-5 (-0.10) / -14 (-0.23)
20	CNRM	-13 (-0.41) / -17 (-0.25)	-7 (-0.07) / -34 (-0.24)	-7 (-0.20) / -12 (-0.18)	-15 (-0.88) / -9 (-0.22)	-21 (-0.51) / -25 (-0.38)
22	HadCM3M2	-16 (-0.41) / -19 (-0.33)	10 (0.09) / -37 (-0.31)	-12 (-0.35) / -14 (-0.26)	-21 (-1.02) / -13 (-0.35)	-18 (-0.35) / -26 (-0.41)
25	HadCM3M2-veg	-24 (-0.60) / -28 (-0.46)	-9 (-0.07) / -48 (-0.39)	-22 (-0.59) / -25 (-0.42)	-27 (-1.26) / -19 (-0.49)	-25 (-0.46) / -35 (-0.52)
MME-all		-20 (-0.60) / -21 (-0.41)	-14 (-0.17) / -36 (-0.32)	-16 (-0.51) / -20 (-0.39)	-21 (-1.08) / -15 (-0.46)	-26 (-0.65) / -27 (-0.48)
MME-PMIP1-SST-f		-27 (-0.79) / -24 (-0.48)	-21 (-0.25) / -37 (-0.32)	-21 (-0.65) / -21 (-0.44)	-25 (-1.24) / -18 (-0.56)	-41 (-1.01) / -31 (-0.58)
MME-PMIP1-SST-c		-15 (-0.48) / -19 (-0.38)	-11 (-0.16) / -35 (-0.31)	-13 (-0.44) / -19 (-0.39)	-17 (-0.93) / -12 (-0.41)	-14 (-0.39) / -22 (-0.40)
MME-PMIP2		-17 (-0.47) / -21 (-0.35)	-2 (-0.02) / -40 (-0.31)	-13 (-0.38) / -17 (-0.29)	-21 (-1.05) / -14 (-0.35)	-21 (-0.44) / -29 (-0.44)

568 *MME-all denotes the ensemble mean of the 15 models; MME-PMIP1-SST-f denotes the ensemble mean of the six PMIP1 SST-f models; MME-PMIP1-SST-c denotes the ensemble mean of the six PMIP1 SST-c models; and MME-PMIP2 denotes the ensemble mean of the three PMIP2 models.

570 Table 5. Proxy data providing estimates of LGM–present changes in annual surface temperature (ΔT_{ann}; units: ^{o}C) in the Chinese mainland

Site	Proxy data	Region	ΔT_{ann}	Reference
12 sites in South China	Pollen	20–32°N, 105–120°E	-7 ± 3.5	Farrera et al. (1999) and references therein
Tianyang Lake borehole	Pollen	20.31°N, 110.18°E	-5 to -8	Zheng et al. (1999)
Seven sites in the Qinghai-Tibetan Tibetan	Ice core, pollen, and sand wedge	28–36°N, 80–100°E	-6 to -9, with an average of -7	Shi et al. (1997), Shi (2002), and references therein
Seven sites in the eastern Qinghai-Tibetan Plateau	Pollen	30–37°N, 92–102°E	-6	Tang et al. (1998)
Hulu Cave	Stalagmite	32.30°N, 119.10°E	around -8	Wang et al. (2002)
80 sites in North and Northeast China	Pollen	34–50°N, 105–135°E	at least -8 to -10	Liu et al. (1988)
Weinan loess-paleosol sequence	Organism fossil	34.24°N, 109.30°E	-7 to -9	Wu et al. (1994)
Weinan loess-paleosol sequence	Phytoliths	34.24°N, 109.30°E	-6.2 to -6.6	Lu et al. (2007)
Guliya ice cap	Ice core	35.17°N, 81.29°E	colder than -9	Yao et al. (2000)
Two boreholes in the Chaerhan Salt Lake	Halite	36.37–37.12°N, 94.15–96.14°E	-6 to -7	Zhang et al. (1995)
Luanhaizi Lake	Pollen	37.59 °N, 101.35 °E	-4 to -7	Herzschuh et al. (2006)
11 sand deposit sites in northwestern Shanxi Province	Pollen	38–41°N, 111–113°E	-9.6 to -15.5	Su and Ma (1997)
Six sites in Hexi Corridor	Sand wedge	39–41°N, 94–100°E	-13 to -15	Wang et al. (2001)

Table 6. Model-data comparison of ΔT_{ann} (units: ^{o}C) in four regions of the Chinese mainland*

Reconstructions and experiments	ΔT_{ann} in each region			
	South China	Qinghai-Tibetan Plateau	Hexi Corridor	North and Northeast China
Reconstructions	-7.0 ±3.5	-6 to -9	-13 to -15	at least -8 to -10
MME-all	-3.39 (*1.77*)	-5.05 (*2.46*)	-4.68 (*1.47*)	-4.86 (*1.92*)
MME-PMIP1-SST-f	-2.23 (*1.30*)	-4.07 (*1.39*)	-3.89 (*1.16*)	-3.67 (*1.50*)
MME-PMIP1-SST-c	-4.77 (*1.89*)	-5.81 (*3.47*)	-5.68 (*1.57*)	-6.40 (*1.84*)
MME-PMIP2	-3.48 (*0.89*)	-5.56 (*1.68*)	-4.65 (*0.99*)	-4.82 (*1.14*)
HadCM3M2	-3.46	-5.94	-4.66	-4.58
HadCM3M2-veg	-4.71	-8.99	-5.77	-7.10

*MME-all denotes the ensemble mean of the 15 models; MME-PMIP1-SST-f denotes the ensemble mean of the six PMIP1 SST-f models; MME-PMIP1-SST-c denotes the ensemble mean of the six PMIP1 SST-c models; and MME-PMIP2 denotes the ensemble mean of the three PMIP2 models. The regions are defined as follows: South China (20–33^{o}N, 105–120^{o}E), Qinghai-Tibetan Plateau (28–37^{o}N, 80–102^{o}E), Hexi Corridor (39–41^{o}N, 94–100^{o}E), and North and Northeast China (34–50^{o}N, 105–135^{o}E). Oceanic regions and land regions not belonging to China are excluded when regionally-averaged value is calculated in each region. The standard deviation (units: ^{o}C) of model results is in italic and given in brackets.

Figure captions:

Figure 1. LGM–baseline changes in annual surface temperature (units: ^{o}C) for (a) the ensemble mean of the 25 PMIP simulations, (b) the ensemble mean of the 10 PMIP1 SST-f simulations, (c) the ensemble mean of the eight PMIP1 SST-c simulations, and (d) the ensemble mean of the seven PMIP2 simulations. Areas with the confidence level below 95% are shaded. Here statistical significance is assessed by the use of a Student *t*-test applied to differences between the LGM and baseline simulations. Regionally-averaged changes within the Chinese mainland are given in brackets.

Figure 2. Percentage changes in annual precipitation (units: %) during the LGM, with reference to baseline climate, for (a) the ensemble mean of the 15 PMIP models, (b) the ensemble mean of the six PMIP1 SST-f models, (c) the ensemble mean of the six PMIP1 SST-c models, and (d) the ensemble mean of the three PMIP2 models. Areas with the confidence level above 95% are shaded. Regionally-averaged percentage changes within the Chinese mainland are given in brackets.

Figure 3. Same as Figure 2, but for percentage changes in annual evaporation (units: %).

Figure 4. LGM–baseline changes in annual P–E (shade, units: mm/day) for (a) the ensemble mean of the 15 PMIP models, (b) the ensemble mean of the six PMIP1 SST-f models, (c) the ensemble mean of the six PMIP1 SST-c models, and (d) the ensemble mean of the three PMIP2 models. Also shown is the lake status-based reconstruction of changes in water balance during the LGM (Yu et al., 2003), in which open squares represent drier conditions, open circles represent wetter conditions, and open stars represent normal conditions.

Figures:

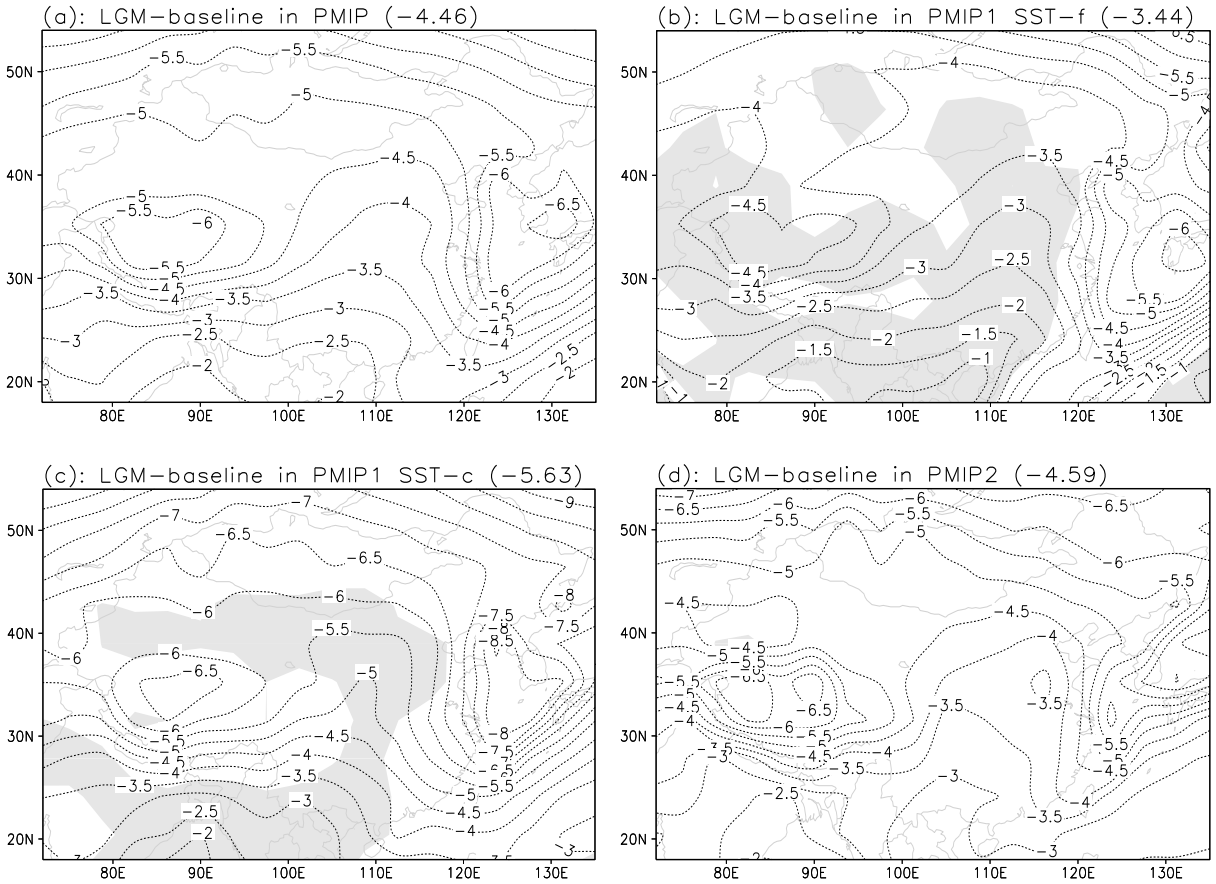

Figure 1. LGM–baseline changes in annual surface temperature (units: ^{o}C) for (a) the ensemble mean of the 25 PMIP simulations, (b) the ensemble mean of the 10 PMIP1 SST-f simulations, (c) the ensemble mean of the eight PMIP1 SST-c simulations, and (d) the ensemble mean of the seven PMIP2 simulations. Areas with the confidence level below 95% are shaded. Here statistical significance is assessed by the use of a Student *t*-test applied to differences between the LGM and baseline simulations. Regionally-averaged changes within the Chinese mainland are given in brackets.

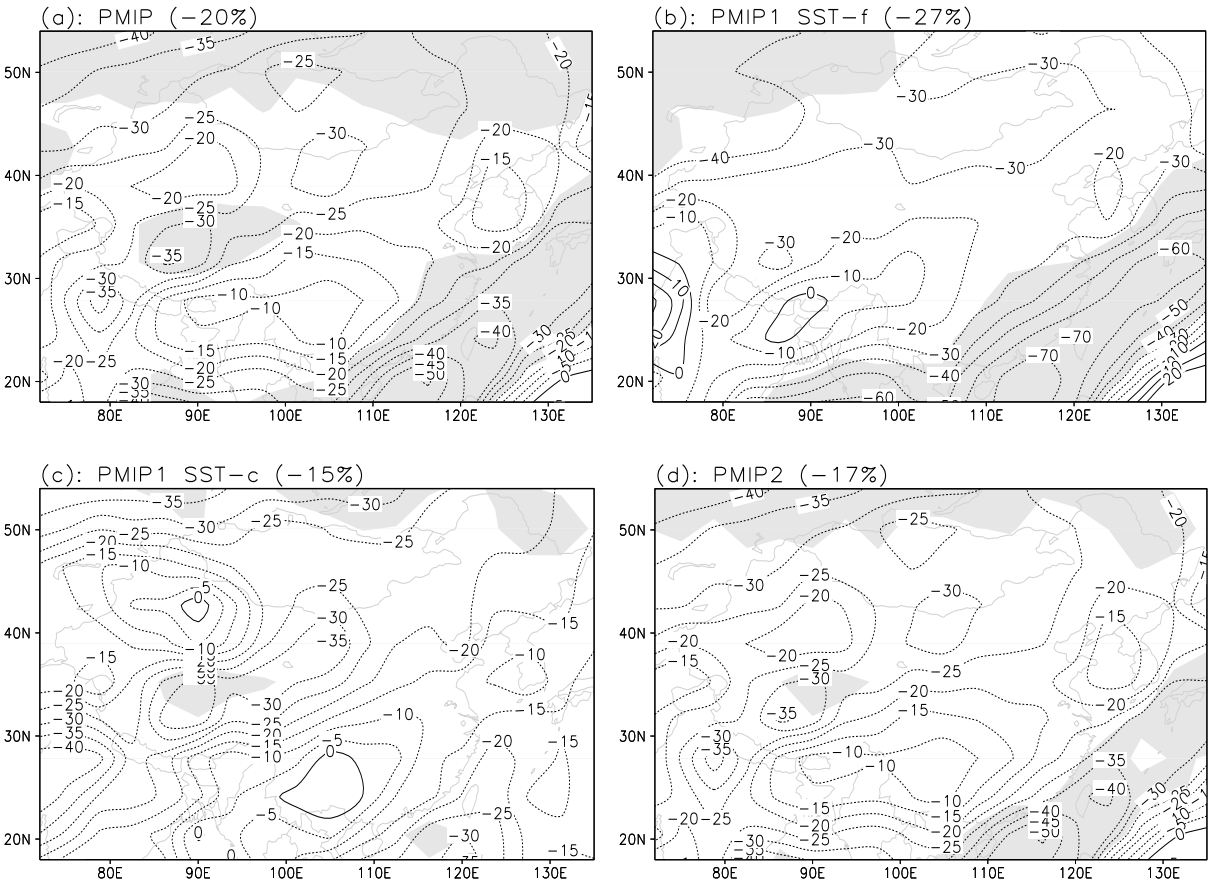

612

Figure 2. Percentage changes in annual precipitation (units: %) during the LGM, with reference

614 to baseline climate, for (a) the ensemble mean of the 15 PMIP models, (b) the ensemble mean of the six PMIP1 SST-f models, (c) the ensemble mean of the six PMIP1 SST-c models, and (d)

616 the ensemble mean of the three PMIP2 models. Areas with the confidence level above 95% are shaded. Regionally-averaged percentage changes within the Chinese mainland are given in

618 brackets.

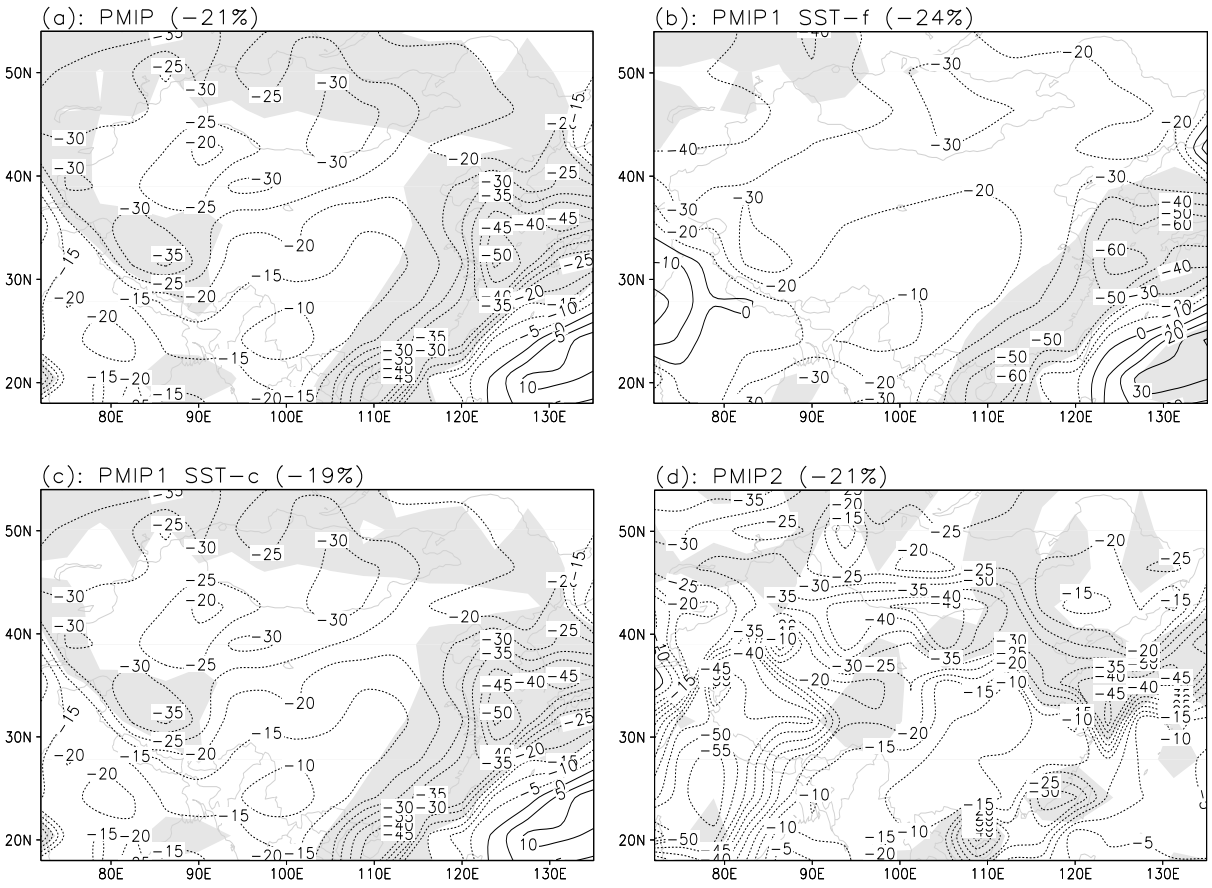

Figure 3. Same as Figure 2, but for percentage changes in annual evaporation (units: %).

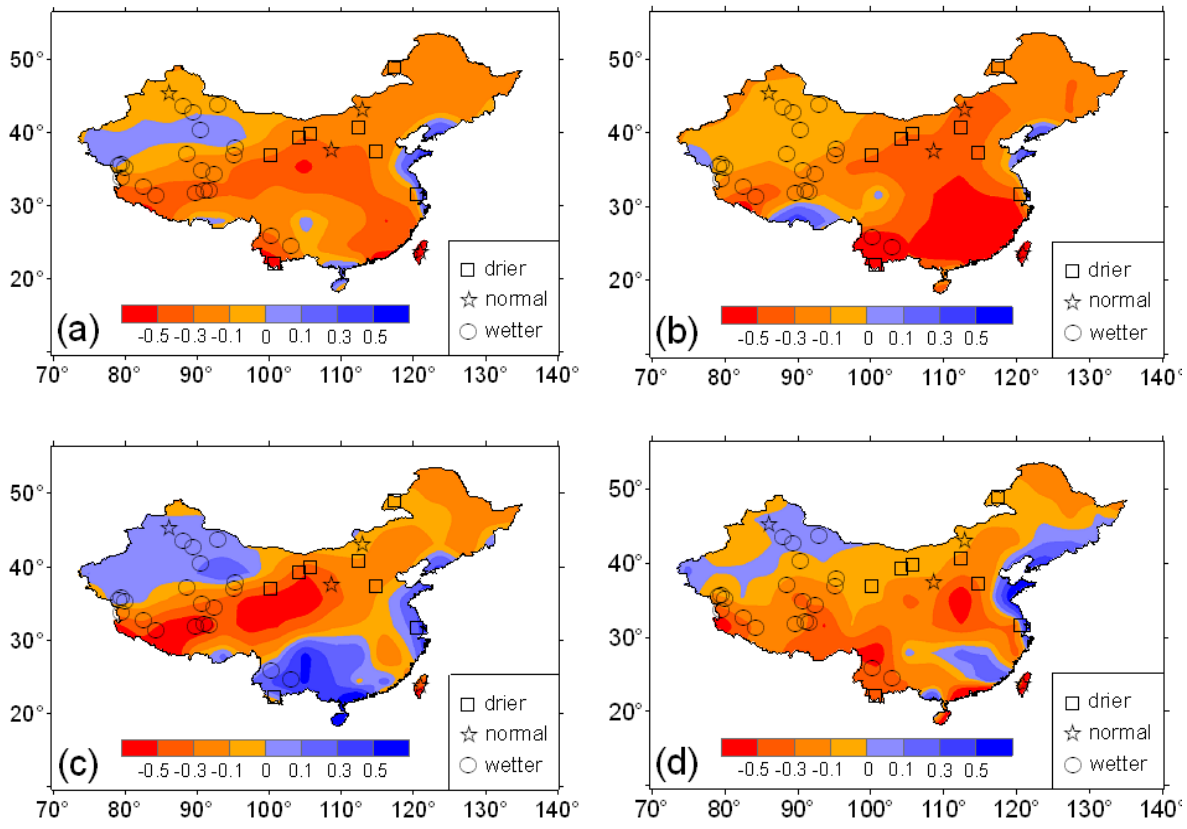

Figure 4. LGM–baseline changes in annual P–E (shade, units: mm/day) for (a) the ensemble mean of the 15 PMIP models, (b) the ensemble mean of the six PMIP1 SST-f models, (c) the ensemble mean of the six PMIP1 SST-c models, and (d) the ensemble mean of the three PMIP2 models. Also shown is the lake status-based reconstruction of changes in water balance during the LGM (Yu et al., 2003), in which open squares represent drier conditions, open circles represent wetter conditions, and open stars represent normal conditions.